SMiRT-12 / K. Kussmaul (Editor)
1993 Elsevier Science Publishers B.V.

U07/2

CORVIS: INVESTIGATION OF LWR LOWER HEAD FAILURE MODES - EXPERIMENTAL PROGRAMME

J. Patorski[1], H. Hirschmann[1] and K. Peters[2]

[1]Programm LWR-Sicherheit, Paul Scherrer Institut, CH-5232 Villigen PSI, Switzerland
[2]Institut für Industrieofenbau und Wärmetechnik, Rheinisch-Westfälische TH, D-5100 Aachen, Germany

ABSTRACT

CORVIS is a research project for the investigation of a possible melt-through of the lower head of the reactor pressure vessel during a core melt accident. Experiments are performed and structural mechanics models of the failure process are developed. This work reports on the status of the experiments. So far several pre-tests have been made, the results of which are presented. We furthermore describe the main experimental facility which is now ready for operation.

1 INTRODUCTION

1.1 Background

One of the current tasks in the research of severe accidents in nuclear power plants is the identification and description of those physical processes which govern the failure of the lower head of the reactor pressure vessel (RPV) when molten core debris relocate to the lower plenum and melt through it. State-of-the-art discussions and computations with respect to this problem have recently been published in the works of Rempe et al. [1] and Bakker [2]. Still missing, however, are experiments on a larger scale which would provide the data necessary to evaluate the computational models available so far. Therefore the research project CORVIS (Corium Reactor Vessel Interaction Studies) was started in 1991 at PSI, the purpose of which is to obtain such data with experiments at atmospheric pressure and thereby to find the dominating phenomena of vessel failure. Carrying out of representative experiments is difficult as far as accident scenarios at elevated system pressure are concerned. In recent probabilistic risk analyses, e.g. [3], the high-pressure path was however found to be the more likely one. Computational models of structural mechanics are therefore developed in parallel to the experiments which make use of the measured data and take into account the material behaviour at high temperatures and also the fluid mechanical behaviour of the melt. Since these models contain the pressure as a parameter, the range of their applicability should also cover the high-pressure path. First results from finite element computations are presented by Duijvestijn et al. [4]. The present work reports on the status of the experimental part of CORVIS.

1.2 General conditions of the melt-through tests

According to the reviews [1] and [2], four modes of lower head failure can be distinguished:
- heat-up and failure of penetration tubes,
- tube ejection,
- lower head global failure,
- jet impingement.

The CORVIS experiments are oriented mainly towards the first two points, but can also provide a limited amount of information on a global lower head failure. The initial condition of the melt-through experiments simulates that stage of a core melt accident, when a pool of molten corium, i.e. molten core material and steel, has already been formed in the still leak-tight lower plenum of the RPV. The experiments are performed at atmospheric pressure thus simulating an accident scenario with low pressure of the reactor coolant system. The following phenomena which characterize the process of heat-up and failure of the lower head will be measured or qualitatively registered:
- Heat-up of the vessel wall and temperature dependent deformations due to the weight of the structures and of the melt,
- the place of a first melt release from the test vessel, i.e., melt-through of the penetration tubes above the welded joints to the vessel wall or failure of the welded joints or failure of the vessel wall;
- the type of vessel leakage, i.e., growth of a single hole or formation of further holes or a large break in the vessel wall;
- the rate and constitution of the melt released from the vessel;

• a possible re-freezing of the melt inside the tubes and tube blockage;
• a possible re-freezing of the melt outside the tubes below the vessel, which partially would inhibit a fast release of a large mass into the reactor cavity.

The test vessel is always a cylindrical steel container, the bottom of which represents a cut-out of the RPV-wall and can carry tube-like insertions. The side wall of the cylinder does not represent any reactor-typical structure. In order to facilitate the measurements and to simplify interpretation, the inner surface of the side wall is thermally insulated with a heat-resistant MgO-based thermal insulation (Magnesital).

The substitute for the corium melt is produced with a thermite charge. Thermite is a commercially available mixture of granulate aluminium metal and iron oxides. During the strongly exothermic thermite reaction, the melt of iron and aluminium oxide can reach a temperature of about 2300°C . However, to simulate a melt-through, as caused by the decay heat during an accident, additional heating of the melt is necessary in the experiments with a full-scale thickness of an RPV-wall model. (For more details about the experimental set-up see section 3.)

2 PILOT EXPERIMENTS OBSERVING VESSEL MELT-THROUGH

Preliminary tests have been carried out with a simplified experimental set-up and small melt charges. We report in the following on these pilot experiments. The purpose of the tests was to get experience for an appropriate design of the main test facility and the measurement techniques as well as to install the appropriate analytic tools for the simulation of the experiments with the method of finite elements (FEM). Computations of transient heat conduction had been made in advance of the experiments; they predicted that, for given boundary conditions, the thermal energy stored in the thermite melt would be able to melt through a vessel bottom plate with a thickness of at least 35 mm. Also these computational results were to be verified with the pilot experiments.

2.1 Experimental set-up

Fig. 1 is a view of the pilot experiment facility. The test vessel is supported by 3 steel rods so that the vessel bottom is 1500 mm above a melt catcher placed on the floor. Inductive transducers protected by metal boxes are placed below the vessel on a horizontal reference beam which itself is fixed to the side wall of the vessel. The test vessel is a steel (St37) cylinder of 500 mm of height, an outer diameter of 508 mm and a wall thickness of 20 mm. The wall was thermally insulated at its inner surface with a 50 mm thick layer of Magnesital so that the free inside diameter was 368 mm. A flat bottom

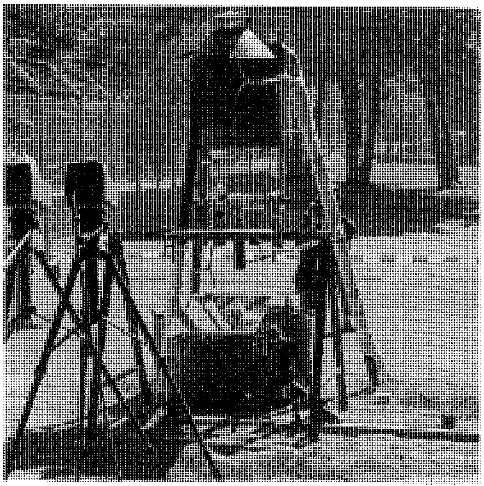

Figure 1: Pilot experiment facility.

plate of plain low carbon steel (St37) was welded to the cylinder wall. Thermite charges of 90 kg were loaded and then ignited in the test vessels. The thermite reaction produced a melt of about 46.8 kg of iron and 43.2 kg of aluminium oxide, which after the segregation of the components, formed melt layers with thicknesses of 59 mm (iron, collecting at the vessel bottom) and 169 mm respectively.

Thermocouples and inductive transducers measured

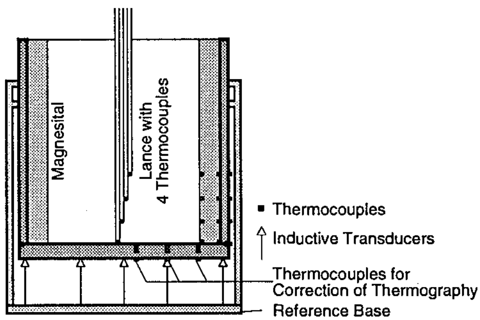

Figure 2: Location of points for measurement of the temperatures and displacements (schematic).

the temperatures and deformations at different places as shown in Fig. 2 . Thermocouples of type K (NiCr/Ni) were inserted inside and outside of the bottom plate, inside the Magnesital insulation at two different depths and at the outer cylinder wall. Additional thermocouples were placed at the horizontal reference base beam, which supported the transducers. A lance with 4 thermocouples of type S (W5Re/W26Re), with tantalum sheaths, was constructed in order to measure the temperature of the melt at different levels and thereby also the propagation velocity of the thermite reaction. Inductive transducers registered the vertical deflection of the vessel bottom at different radii. Each transducer coil was mounted (in shielding boxes) on the reference beam and the sliding anchor was suspended through a thin ceramic rod (Al_2O_3) and a short piece of tungsten wire (length: 10 mm) at the bottom plate. This wire connection is temperature resistant and it is flexible in order to prevent a transfer of bending forces to the coil. The transducer data were corrected for the thermal deflection of the reference base with the help of the measured temperatures. For the data acquisition of the point-like measurements, the two scanning systems UPM60 and UPM100 from HBM Darmstadt were tested, the latter giving a repetition frequency of 2.24 Hz per channel with 40 input channels.

In addition, the temperature field at the outer surface of the bottom plate was registered by infrared thermography. The IR-camera recorded the pictures of the bottom surface via a metallic mirror placed outside and below the test section. (See Fig. 1.) The data were collected by a special processing unit for thermography and stored on the RAM disk of a computer. The Thermoflir System Type 6200 was used for the thermography measurements. With this system, a frequency to build up a complete picture (frame frequency) of 2 Hz was achieved, which is similar to the frequency of the point measurements. The spatial resolution typical for the experiments corresponds to a 6.35 x 4.4 mm field of the object surface from which the emitted energy is integrated by the process unit.

Thermography technique is based on an integration of Plank's radiation law. The emissivity factor appearing there has to be estimated in order to interpret the radiation pattern received by true temperatures. The emissivity generally depends on the wavelength, the surface conditions (e.g. the degree of oxidation) and the temperature. Since the emissivity varies throughout the object surface and also in time it is not possible to tune the thermography apparatus to immediatly detect and provide the correct temperatures. Therefore a correction of the raw thermography data was made using the data from a set of 3 thermocouples attached to the surface. The temperatures measured with these thermocouples are assumed to be correct. For each thermocouple, the difference to the thermographical temperature detected at the same place (at arbitrary time) is associated with this temperature. For a fixed thermographical temperature, the 3 thermocouples will yield slightly scattered difference values which can be interpreted as the uncertainty of the correction. In this way, a correction and also an uncertainty interval (called experimental scatterband), can be associated to each thermographical temperature. This method is also appropriate to correct for other distortions caused by a reduced optical quality of the mirror, absorption by the atmosphere or reflection from other surfaces. The procedure to correct thermographical raw data is documented in [5].

2.2 Results from the pilot experiments

Three pilot experiments were performed with bottom plates of 25 and 35 mm of thickness and after different drying times of the Magnesital insulation (see Table 1). The heat-up of the thermite after ignition was

Table 1: Experimental parameters

Experiment number	Bottom plate thickness [mm]	Melt-through Time [s]	Melt-through Location	Magnesital technol. water wg.cont. [%]	Magnesital Drying time [day]
0/1	25	54	centre	4	3
0/2	35	65	edge	6	3
0/3	35	125	edge	5	14

detected with the lance (4 thermocouples) at different heights. Fig. 3 shows the temperatures measured in the time between ignition of the thermite and the failure of the thermocouples. All thermocouples survived for about the same time interval of 2 s after the arrival of the thermite reaction front, until failure. The maximal temperature observed was 2320 °C , which is close to the assumed boundary conditions in [4]. According

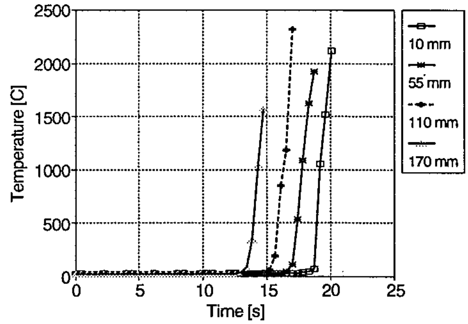

Figure 3: Melt temperatures vs. time at four heights from the bottom plate along the lance on the central axis of the vessel. (Exp. 0/3)

to the observed times, the vertical propagation velocity of the reaction is 32 mm/s. The reaction reached the vessel bottom after 15 s; this was confirmed by the thermographical measurement which showed a temperature rise at the same time (see [5]).

In all experiments, the iron melt attacked the bottom and finally melted it through. Two shapes of destruction of the bottom were found, as shown in Fig. 4. A central hole was melted into the 25 mm bottom plate (experiment 0/1), the remaining parts of the plate being cambered upwards. The resulting concave shape of

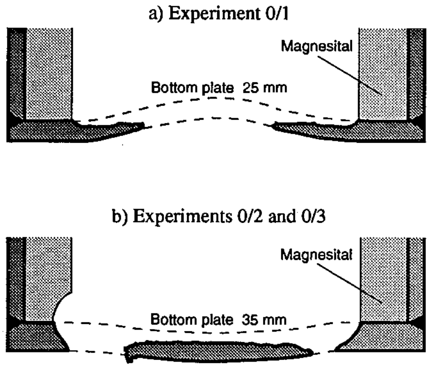

Figure 4: Damage forms. Vessel cross-sections with melted-through bottom plate.

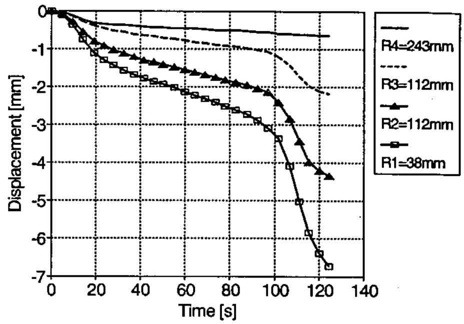

Figure 5: Displacements of the bottom plate vs. time at four points at different radial distances from the centre. (Exp. 0/3)

the plate in experiment 0/1 may be due to a combined action of buckling and thermal expansion loads. The plates with a thickness of 35 mm (experiments 0/2 and 0/3) showed a toroidal wash-out which also was continued into the Magnesital layer. We presently suppose that mainly a violent release of water vapour and other gases (e.g. hydrogen) from the Magnesital promoted a toroidal vortex near the bottom which enhanced the heat flux from the melt into the metal and at the same time eroded the Magnesital. This interpretation is supported by the fact that the content of residual water was smallest in experiment 0/1 so that a strong gas-driven convection could not be established. Comparing experiments 0/2 and 0/3, the water content is also significant to the total duration till bottom plate melt-through; the smaller the water content, the longer the time to failure. In future experiments, the water content of the insulation has to be minimized in order to suppress the presumed gas-driven convection. In contrast to 0/1, experiments 0/2 and 0/3 resulted in downwards directed displacements of the bottom plate. Fig. 5 shows the vertical displacements measured at four different places with distances from the vessel axis R1,...,R4 (distance R2 equals R3, but their places are lying opposite of the axis). The downwards displacement of the point nearest to the axis (radius R1) is largest at any time which indicates that the deformation of the bottom plate had always a convex shape. Axial symmetry of the displacement field was not conserved throughout the whole measurement; this is indicated by the asymmetric displacements at the two measuring points with the equal radii R2=R3. After about 100 s, a strong change in the displacement velocity is observed; for instance, at the point with R1, the velocity changes from 0.02 mm/s to 0.16 mm/s. According to the thermographical measurement, the whole outer surface of the bottom plate had reached a temperature of more than 700 °C at this time. The rapid increase of the displacement velocity may therefore partially be explained by a decrease in the strength of the steel at this temperature, but the effect is also enhanced by the removal of material due to erosion near the wall.

The application of thermography has certain advan-

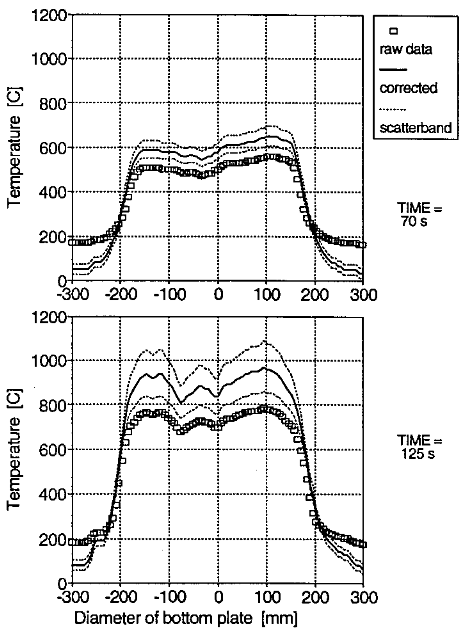

Figure 6: Thermography temperature profile along the diameter (90°–270°) on the outer surface of the bottom plate at times 70 s and 125 s after ignition. Comparison of raw thermography and corrected values.(Exp.0/3)

tages over the point-like measurements with thermocouples, i.e. the visualisation of the full temperature distribution - dependent on time - over the whole surface of the test object and the detection of hot spots. The measurement is quantitative and therefore can provide data necessary for the verification of computational failure models with the methods of structural mechanics. As mentioned in section 2.1, the thermographically measured raw temperatures have been corrected with respect to the emissivity and other distortions using thermocouple data. As an example, Fig. 6 shows the raw and the corrected temperature profiles along a fixed diameter (90°–270°) of the bottom surface at the times 70 s and 125 s respectively. Also shown are the upper and lower limits of the uncertainty band of the corrected temperature. The uncertainty increases with temperature because the emissivity becomes increasingly more inhomogeneous at the surface. Therefore the uncertainty band is larger at the detection time of 125 s - just before the beginning of the plate failure. Fig. 7 shows

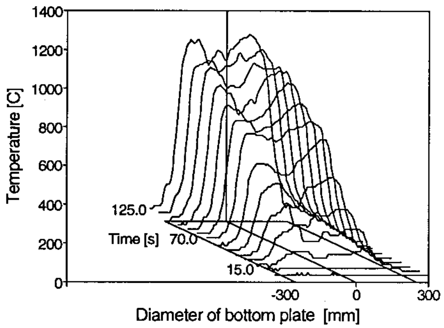

Figure 7: Thermography transient temperatur profiles along the diameter (90°– 270°) on the outer surface of the bottom plate up to melt-through time 125 s after ignition. (Exp.0/3)

in 3D-manner the profile of corrected thermographical temperatures along a fixed diameter at the vessel bottom (experiment 0/3) for the whole time range of the experiment. It can be clearly seen that at about 15 s the temperatures at the outer parts of the bottom start to rise faster than those at the centre. This is in good agreement with the finally observed failure mode as shown in Fig. 4 b).

The differences of the temperature profiles of Fig. 8, along four orthogonal radii indicate that the melting process was not axially symmetrical. This may be a randomly initated effect which however lasts after initialisation and becomes more distinct with increasing temperature. The analysis of this effect may be a challenge for a probabilistic investigation with 2D-symmetrical models using stochastic mechanics.

3 MAIN TEST FACILITY

The main experimental facility for larger experiments has been designed and constructed using the experience

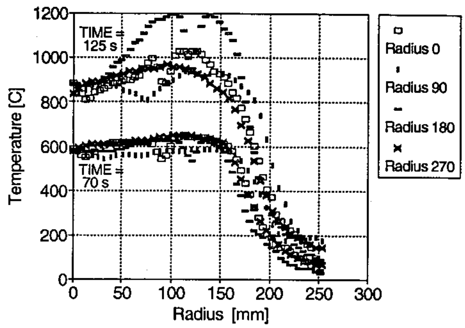

Figure 8: Comparison of temperatur profiles of four orthogonal radii on the outer surface of the bottom plate at time 70 s and 125 s after ignition. (Exp.0/3)

from the pre-tests. Schematic and real views are presented in Figs. 9 and 10 respectively. Construction details are in [6] .

3.1 Test Facility with DC Arc Heating

Test section: The central part of the set-up is the experimental vessel (Fig. 9). It is a cylindrical steel container, the bottom of which represents a cut-out of an RPV lower head wall. Tube-like penetrations can be inserted into the bottom with a reactor-typical welding technique. The scale of the bottom thickness and of the penetrations is 1:1 (Thickness: 100 - 120 mm. Free diameter of the bottom: 600 - 900 mm). A number of slices of reactor steel (20 MnMoNi 55) was provided by the Staatl. Materialprüfungsanstalt Stuttgart. As in the pre-tests the cylindrical part is only the carrier of the bottom; it is thermally insulated inside with Magnesital. Below the bottom, a space of 5 m height is available. Long continuations (as encountered in several reactor designs) of the tube penetrations can be joined there in order to observe a possible re-freezing of the melt at these structures outside of the vessel. The whole set-up is axially symmetric in order to facilitate a later analysis of the experiments in axisymmetric geometry.
Magnesital is a water-poor, quickly setting concrete with 92.5% MgO, 3.6% SiO_2, 1% Cr_2O_3, and earth-alkali oxides. Long-term heat resistance: 1700°C .

Thermite reaction vessel: The melt mass representing the reactor core melt is produced with a thermite charge. In order to achieve well-defined initial conditions for the experiments, the thermite is ignited in a seperate reaction vessel (capacity: 2000 kg of thermite). In this way the turbulent phase of the thermite reaction is excluded from the experiment and a sufficiently large melt mass can be filled into the experimental vessel. According to our analyses, the available thermite mixture contains

two iron oxides, so that both the reactions:
$3Fe_3O_4 + 8Al \rightarrow 9Fe + 4Al_2O_3 + 3676$ kJ/kg
(main reaction) and
$Fe_2O_3 + 2Al \rightarrow 2Fe + Al_2O_3 + 3990$ kJ/kg
take place. The water content is less than 0.1%. For safety reasons, the charge is still dried out for several days before the ignition. Hot gases produced during the reaction are removed by a ventilation (capacity:4m^3/s).

Pouring channel: An automatically controlled channel is used to pour either the metallic or the oxidic melt component (or both) from the reaction vessel into the experimental vessel.

Electrical arc heater: As is known from preliminary computations, the heat losses of the melt, as soon as it is filled into the experimental vessel, are much too high to melt through the bottom with the stored energy alone. Therefore a DC-driven electric arc heater was installed for a sustained heating of the melt in the test section (see detail of Fig. 9). The arc burns between the lower ends of two concentric graphite electrodes in an atmosphere of argon gas. By lowering the electrodes and pressurizing the gap between them, the heat source (i.e. the arc) can be positioned at an arbitrary level below the surface of the melt pool. This method of electric heating with a movable hot zone of small extent has recently been developed at the Institut für Industrieofenbau und Wärmetechnik im Hüttenwesen der RWTH Aachen, Germany. The arc heater at PSI will provide a maximum power of 300 kW.

3.2 Instrumentation

The instrumentation is planned to register quantitatively all phenomena listed in section 1.2. Two classes of sensors will be used,

- contact type sensors as thermocouples, inductive transducers and load cells with strain gauges,
- optical instruments as infrared cameras, pyrometers and video recording.

Thermocouples will be distributed on the experimental vessel in a similar way as in the pre-tests in order to provide data which give a precise pattern of the thermal loads. This pattern is completed by the dense field of thermographical data. Inductive transducers will register the displacements of the bottom plate in both the vertical and the horizontal direction. With the load cells positioned below the experimental vessel, the melt basin and also the thermite reaction vessel will register the rates of melt transport. The pyrometers, based on dual-wavelength technique, measure the temperature of the melt.

The data acquisition for all data of the point measurements and of several control signals will be done with a HP3852A Data Acquisition/Control Unit, a 13-bit High-Speed Voltmeter HP44702B (Hewlett-Packard) and other HP components. The HP3852A communicates with a HP1000/900A computer. Together with the software written at PSI a scanning frequency of about 10 Hz per channel can be achieved for 100 input channels. The infrared thermography will be performed independently with its own computer. The achieved frame frequency is 25 Hz.

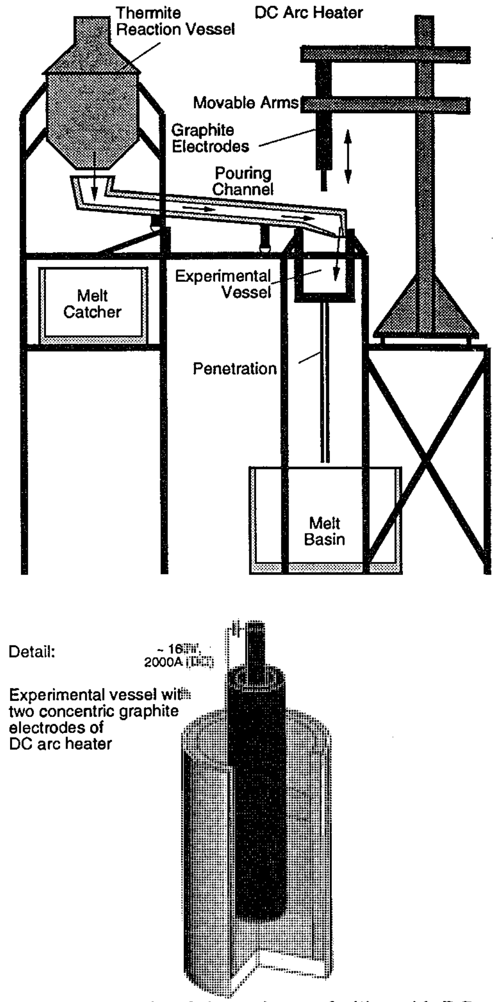

Figure 9: Schematic of the main test facility with DC arc heater.

CONCLUSIONS

Preliminary experiments have been successfully performed to observe melt-through of a steel container in contact with a thermite melt. Temperature and displacement data of this process have been taken using different sensors and measuring principles. Experience was gained during these tests to design a larger experimental

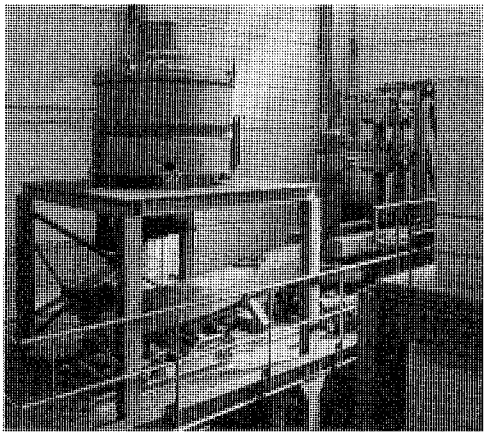

Figure 10: Realization of the CORVIS main test facility at PSI. Foreground: Thermite reaction vessel. Below: Pouring channel. Background: Electric DC arc heater.

facility, which in the mean time has been established at PSI. First experiments with the fully instrumented new set-up will be performed during the year 1993. They will provide insights in specific failure mechanisms as well as data for the verification of the computational model developed at PSI to asses numerically RPV lover head failure.

ACKNOWLEDGEMENTS

We are grateful to the management of the Paul Scherrer Institute for initiating and guiding CORVIS. We also thank the Swiss Federal Nuclear Safety Inspectorate (HSK) and the Swiss Federal Office of Energy (BEW) for supporting this project. Our best thanks going to the Kernforschungszentrum Karlsruhe in Germany for valuable consultations. Our special thanks go to Prof. Dr.-Ing. H. Wilhelmi and his team from the Institut für Industrieofenbau und Wärmetechnik im Hüttenwesen der RWTH Aachen, Germany for fruitful cooperation. We also thank the Staatliche Materialprüfungsanstalt (MPA) in Stuttgart, Germany for donating the reactor-steel. The authors thank Mr. Chr. Florin and his team from the Flir AG company in Kriens, Switzerland for assistance in the recording of thermograpy measurements. Special thanks are due to the international CORVIS task force and many colleagues in PSI for scientific and technical assistance. We like to thank Mr. R. Attinger (now NPP Gösgen) for his engagement in the first phase of the project.

REFERENCES

[1] Rempe J. L. et al. (1992), "Light Water Reactor Lower Head Failure Analysis" (Draft), NUREG/CR-5642, EGG-2618 March 1992

[2] Bakker P.J.T. (1992) "State of the art report for reactor pressure vessel bottom head failure", KEMA Report 20111-WMK-1, Arnhem, Netherlands.

[3] Gesellschaft für Reaktorsicherheit (1990), "Deutsche Risikostudie Kernkraftwerke Phase B. Eine Untersuchung im Auftrag des Bundesministers für Forschung und Technologie" Köln, Germany, Verlag TÜV Rheinland

[4] Duijvestijn G., Rösel R., Brosi S., (1993), "CORVIS: Investigation of LWR Lower Head Failure Modes, Computational Analysis of Structural Behaviour", Proc. of 12th International Conference on Structural Mechanics in Reactor Technology Transactions, Division U, Stuttgart, Germany.

[5] Patorski J. (1992), "Dynamic surface temperature measurement developed for the CORVIS test program - Thermography", CORVIS-Report Nr.3, Paul Scherrer Institut, Villigen, Switzerland.

[6] Attinger R., Hirschmann H., Kottowski H.M. and Patorski J. (1992) "Test Facility", CORVIS-Report Nr.2, Paul Scherrer Institut, Villigen, Switzerland.